Available online at www.sciencedirect.com

ScienceDirect

Energy Procedia 49 (2014) 295 – 304

Energy Procedia

SolarPACES 2013

Solar thermal power system augmented with LHP

M. Saleem Basha[a], Lalit Bansal[a], Durgesh Sarma[a], Saptarshi Basu[a]*, Pramod Kumar[a], Amrit Ambirajan[b]

[a]*Indian Institute of Science, Bangalore 560012, India*
[b]*ISRO Satellite Center, Bangalore 560017, India*

Abstract

The present work reports the study of the bubble formation dynamics in the compensation chamber (CC) of the evaporator in Loop Heat Pipes. A series of experiments were conducted at different heat loads and bubbles in the CC were visualized. Bubbles diameter, frequency and velocity were measured and correlated against heat loads. Temperatures were measured at various locations and heat transfer coefficient was calculated. Performance of the LHP evaporator was evaluated at different heat loads.

Selection and peer review by the scientific conference committee of SolarPACES 2013 under responsibility of PSE AG.
Final manuscript published as received without editorial corrections.

Keywords: LHP, Solar heating, Bubble

1. Introduction

Heat pipes are heat transport devices capable of transporting high heat fluxes even with minimum temperature difference. Heat pipes are extensively used in heat transfer applications such as electronics cooling, spacecraft thermal control, solar thermal power systems etc due to their simple design (absence of any movable parts), low maintenance and better efficiency. Heat pipe under vacuum provides efficient heat transport capability in solar thermal water heating applications over regular heat exchangers [1-3]. Pumps used in conventional solar power systems can be replaced with loop heat pipes which don't consume energy for development of head. Capillary forces generated in the evaporator because of porous material drive the working fluid, which is responsible for the heat transport. The working fluid undergoes a phase change and the vapor flows towards the condenser through the vapor

* Corresponding author. Tel.: +91-7760808825; fax: +0-000-000-0000 .
E-mail address: sbasu@mecheng.iisc.ernet.in

Selection and peer review by the scientific conference committee of SolarPACES 2013 under responsibility of PSE AG.
Final manuscript published as received without editorial corrections.
doi:10.1016/j.egypro.2014.03.032

line. Upon reaching the condenser, the working fluid condenses back to liquid, returning to the evaporator via the liquid line. Also, the evaporator can be flat plate or cylindrical with vapor grooves. The evaporator is provided with grooves so as to have a better thermal contact between the core and compensation chamber i.e. to allow the heat supplied at the evaporator base to reach the working fluid to facilitate evaporation. The working fluid must be constantly fed into the evaporating region of the compensation chamber.

Conventional heat pipes are provided with a wick all along its length which causes higher pressure drop, so their heat transport capability is limited to short distances. This limitation is overcome in Loop Heat Pipes (LHP) where wick is provided only in the evaporator region. Unlike heat pipe, LHP is provided with the compensation chamber for continuous supply of the working fluid.

Extensive research has been carried out for understanding the steady and transient behavior of LHP with different heat loads and working fluids [4-6], however, the literature in this field lacks on the data of bubble dynamics in the compensation chamber (CC) of the evaporator particularly at high heat loads or catastrophic operating conditions. Evaporation dynamics in a flat plate LHP was studied by Wong et al. [7] and they calculated the evaporator resistance. However, they did not observe any boiling phenomenon in the evaporator. Muraoka et al. [8] simulated bubble generation in the compensation chamber through mathematical modeling to identify the operational limits of LHP. Lin et al. [9] analyzed the flat plate loop heat pipe provided with two compensation chambers and studied the bubble formation at different heat loads. In the present work, bubble dynamics in the CC has been explained in terms of bubble frequency, diameter and velocity at different heat loads and heat transfer coefficient has been evaluated.

Nomenclature

C	specific heat (J/kg-K)
D_p	pore diameter (m)
σ	surface tension (N/m)
g	acceleration due to gravity (m/s^2)
h	heat transfer coefficient (W/m^2-K)
h_{lv}	latent heat of vaporization (J/kg)
K	thermal conductivity (W/m-K)
Nu	Nusselt number
Pr	Prandtl number
q"	heat flux (W/m^2)
ρ_l	density of liquid acetone (kg/m^3)
ρ_v	density of vapor acetone (kg/m^3)
ε	porosity

2. Experimental setup

For the experiment, instead of considering the entire loop heat pipe, only the evaporator is studied. This is because we are interested in studying the operating characteristics and visualise the phenomenon inside the evaporator under unusual or catastrophic loading. Schematic of the optically accessible experimental setup is shown in Fig. 1.

Fig. 2 shows the evaporator in the open loop configuration. Mechanical details of the evaporator are given in Table 1. The liquid inlet pipe is sealed and the vapor is vented out resulting in gradual decay of liquid level in the compensation chamber. Three thermocouples are fixed on the vapor side (i.e., two sensors in between the vapor grooves of evaporator plate and one on the wick on vapor side) through the vapor line. Two thermocouples are fixed on the liquid side (one sensor near the wick and other in the liquid region) (Fig. 3). These two sensors are ensured to be in contact with liquid at all times. Evaporator chamber is bolted to the bottom plate, and subsequently optical windows are assembled.

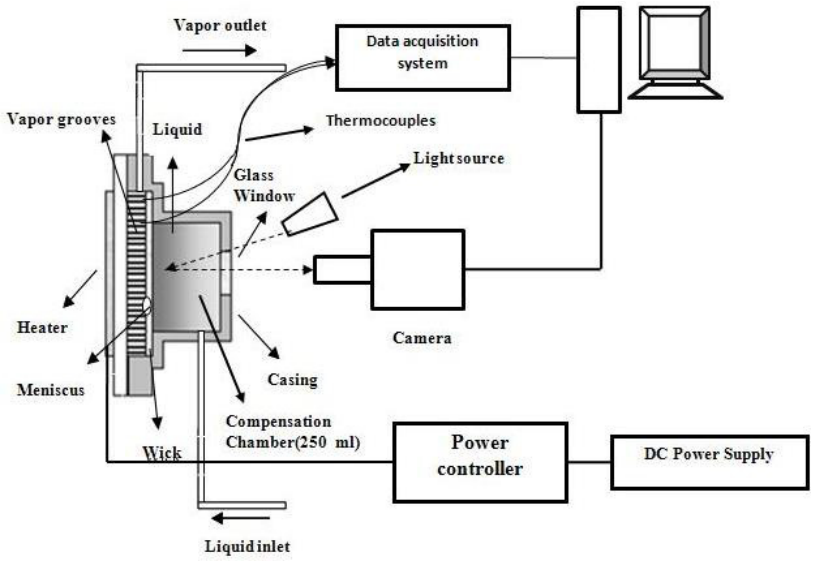

Fig. 1. Schematic of the experimental Setup

An electrical resistance mica heater with a maximum power rating of 60W is fixed on the bottom side of the evaporator plate. The heater is operated with the help of a PID controller, which receives feedback from a thermocouple placed on the heater. Evaporator assembly is completely insulated with glass wool and covered with aluminum foil tape to prevent heat leakage and also to avoid external environmental effects. For visualisation inside the core region of the liquid phase, a window of diameter 44 mm is made and this window is covered with a toughened glass. In addition to this main visualisation window, two additional windows of 20 mm diameter are also arranged to facilitate observation in any desired position of the evaporator. After the assembly of the evaporator and arrangement of thermocouples, a high speed CCD (Redlake-IDT) camera is focussed on a fixed region (region of interest, ROI= 3 mm x 3 mm) on the porous wick throughout the experiment.

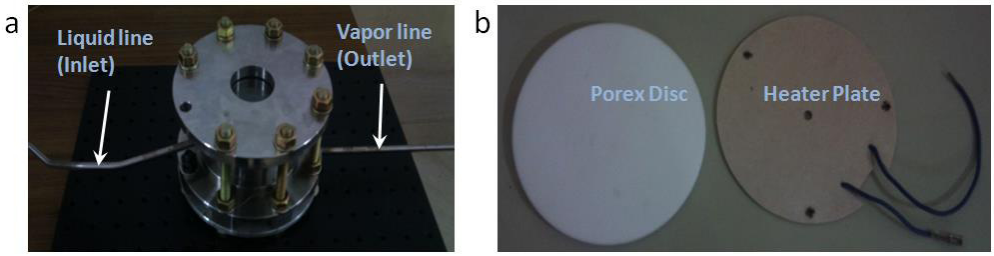

Fig. 2. (a) Evaporator assembly (b) Porous disc and Electrical resistance heater

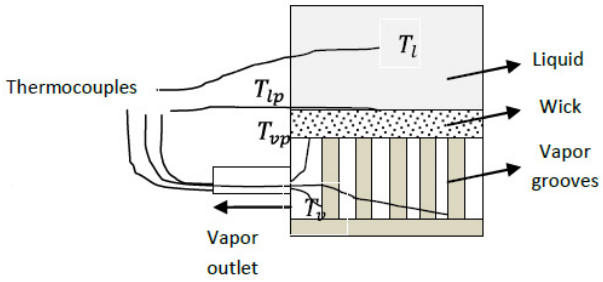

Fig. 3. Arrangement of thermocouples across wick

Table 1. Geometric details of Evaporator

Parameter	Value
Diameter of evaporator CC	84mm
Length of evaporator CC	40mm
Thickness of evaporator CC	5mm
Volume of CC	221cc
Material of CC	SS316
Length of liquid line	150 mm
Length of vapour line	160 mm
Size of liquid/vapour manifold	6.4 mm
Diameter/thickness of porous disc	Φ101mm / 6mm
Material of wick	PVDF
Pore size	15-40 µm
Porosity	0.6
Size of vapour grooves	1 mm^2
Heated area of base plate	25π cm^2

3. Results and discussion

3.1Temperature profile

For our study, temperature is measured at various locations inside the evaporator. These measurements along with their transient variations are recorded using a NI data acquisition system at 10 sample/sec. The temperature profiles obtained for a heater load of 60W are shown in Fig. 4. From the temperature profiles we can observe the regions of convective heating and bubble formation (Nucleate Boiling). Temperatures on the liquid side T_{lp} and T_l increase steadily in the convective heating and nucleate boiling regime and tend to merge in the later stages.

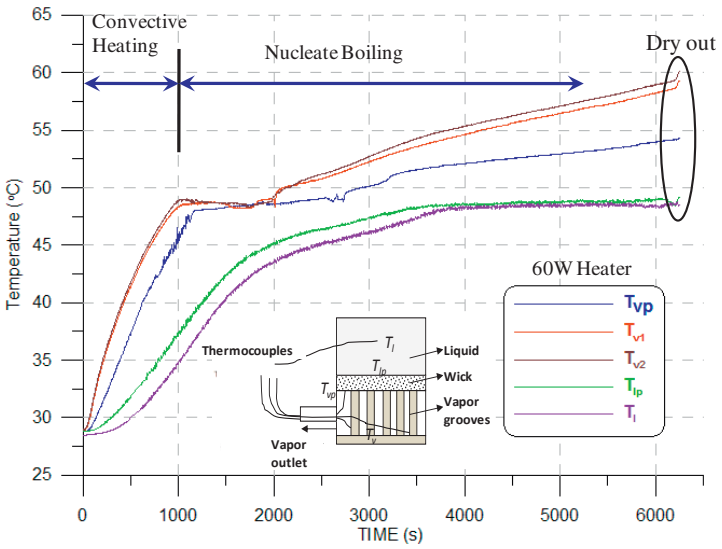

Fig. 4. Temperature profile for heat load of 60W

This is similar to evaporation occuring from a plane surface. Temperature T_{vp} is observed to increase sharply in the convective boiling regime whereas in the nucleate boiling regime, the rise in temperature is gradual. At this junction of transition from convective heating to nucleate boiling, the sharp change in temperature gradient can be observed. Temperatures T_{v1} and T_{v2} also behave similarly, but in the nucleate boiling regime the temperature

gradient is observed to be minimal over a particular time period (isothermal condition). For a heat load of 50W, the temperature profile is found to be almost similar to that of 60W. Fig. 5 shows the temperature profile for heater power of 40W.

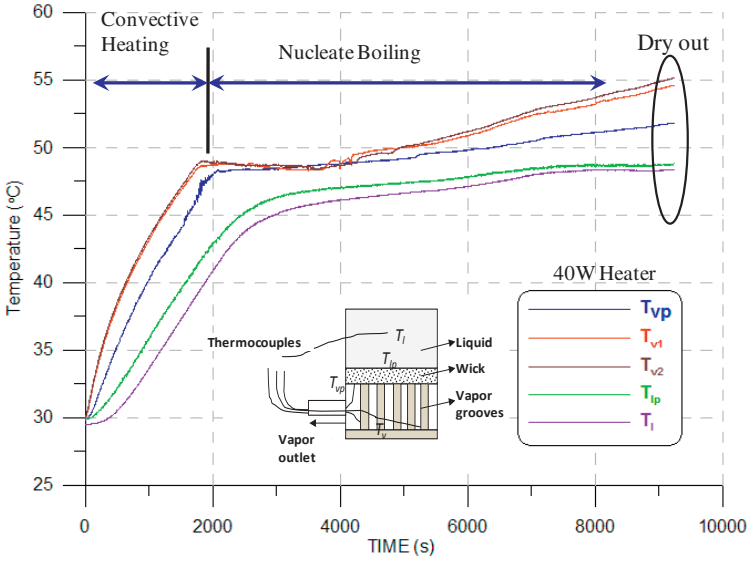

Fig. 5. Temperature profile for heat load of 40W

Both cases (40 W and 60 W) exhibits a gradual increase in temperature on the vapor side after the isothermal condition is achieved. This is because, after certain time from the start of the experiment acetone falls below the critical level in the evaporator core. This is justifiable because mass of working fluid in the compensation chamber is decreases continously whereas the same heat flux is being maintained until the end of the experiment.

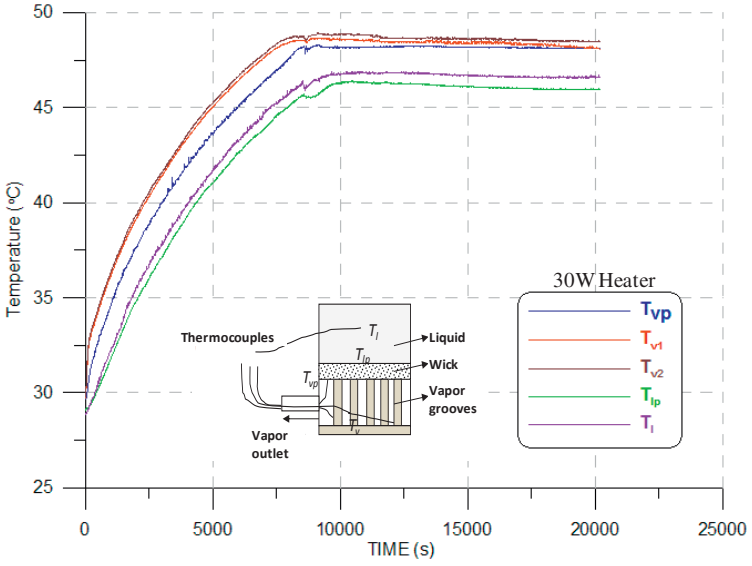

Fig. 6. Temperature profile for a heat load of 30W

Fig. 6 shows the temperature profile corresponding to a heat load of 30W. The phenomenon observed is entirely different from the other heat loads. As usual, all the temperature curves seem to show gradual increase and tend to

reach steady state. The experimentation time is considerably long and even after long time there still seems to be only convection without any boiling. All the temperatures tend to reach isothermal condition. From the variations shown above, this seems to be the lowest heat load as any further reduction in heat load just vaporizes the liquid acetone without any bubble formation. Temperature difference across the wick is plotted against time (Fig. 7).

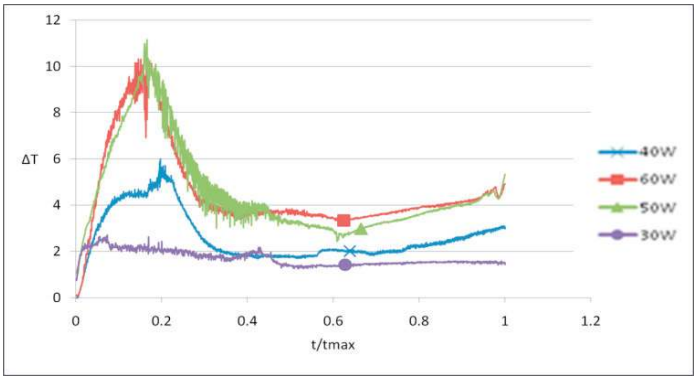

Fig. 7. Temperature drop across the wick

3.2 Calculation of heat transfer coefficient

For transition boiling in porous media, Fukusako et al. [10] recommended the following empirical correlation based on experimental results:

Nussult number,

$$Nu = \frac{q'' D_p}{\Delta T_e K_{eff,l}} = 0.075\left[\frac{D_p}{\sqrt{\sigma[g(\rho_l - \rho_v)]}}\right]^{0.9}\left[\frac{h_{lv}}{C_{eff,l}\,\Delta T_e}\right]^{m} P_r^{2.37}\left[\frac{K_{eff,l}}{K_l}\right]^{n} \tag{1}$$

Where,

$$m = 1.3\left[\frac{D_p}{\sqrt{\frac{\sigma}{[g(\rho_l - \rho_v)]}}}\right]^{0.6} Pr_l^{-0.8} \tag{2}$$

$$n = -0.59\,Pr_l^{0.3} \tag{3}$$

Total heat flux at the teeth-wick interface, $q'' = \frac{Q}{A_t}$ (4)

Effective thermal conductivity of the wick, $K_{eff,l} = \varepsilon K_l + (1-\varepsilon)K_{sm}$ (5)

Effective specific heat of the wick , $C_{eff,l} = \varepsilon C_l + (1-\varepsilon)C_{sm}$ (6)

Heat transfer coefficient, $h = \frac{Nu^* K_{eff,l}}{d}$ (7)

The above correlations are valid for transition boiling only. In fig.8. it can be observed that the heat transfer coefficients increases in nucleate boiling regime and gradually decreases during rapid depletion of acetone in the CC. Initially during the time of nucleate boiling, the wick is completely saturated with liquid and the boiling occurs slowly. The heat transfer coefficient decreases below a particular heat load (50W).

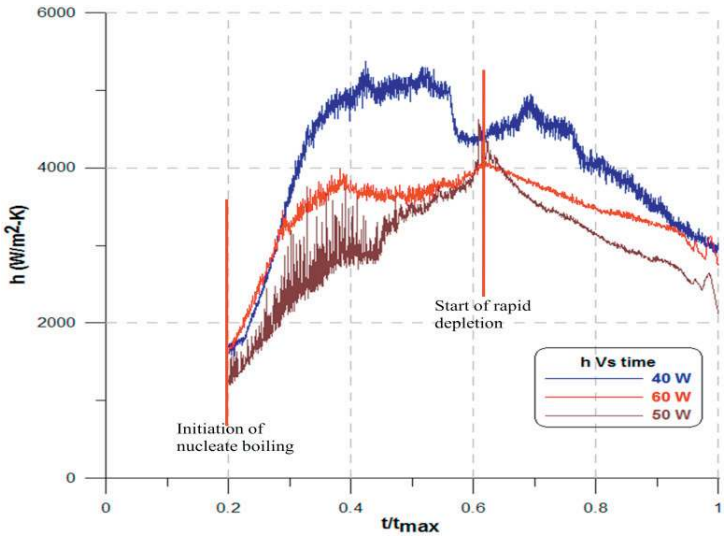

Fig. 8. Variation of heat transfer coefficient across the wick for different heat loads in the nucleate boiling regime

3.3 Bubble visualization

Along with the temperature measurements, bubble formation and movement are visualized. For proper visualisation of bubble formation from the pores, a high speed CCD camera is used. The camera is used along with a 3X zoom lens assembly. After the formation of bubbles, images are captured at around 800 Hz. During the nucleate boiling phase, approximately 800 frames (i.e. around 1 sec) were captured at regular time intervals. The camera is focused on the porous media at a fixed area of 3mm x 3mm. The video captured is split into images (fig. 9) for further processing.

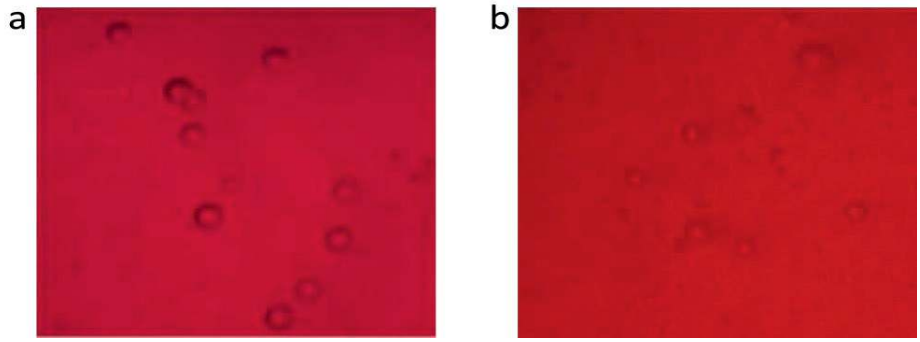

Fig. 9.Captured bubble images

The sequence of images obtained from the video are processed using MATLAB edge detection tool. Bubble diameter and frequency are measured for each heat load. The data is plotted aginst experimentation time.

3.3.1 Bubble frequency

In fig.10, it can be observed that the initial formation of bubbles require some time considering that heat transfer via conduction should take place from the heater plate through the evaporator grooves to the working fluid. Once the first bubble forms, the bubble activity starts to rise and then there is a gradual drop which can be linked to the rapid depletion of the acetone as the system crosses the steady state.

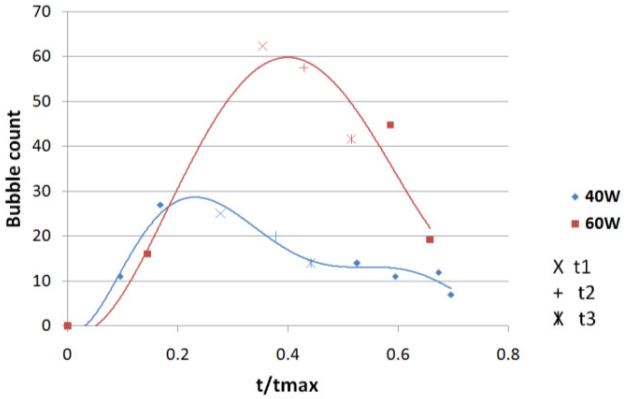

Fig 10. Bubble count for all heat loads normalised with time

t1,t2 and t3 are three time instants selected around the maximum peak that is observed in the frequency plot (fig. 10). Also, by observing both the temperature profiles and frequency plot at the same time, it can be observed that in the convective heating regime bubble frequency tend to be have a nominal value. Actually in the convective heating regime, the bubble formation should not be predominant. But, as per theory there always exist some bubbles in the wick. As the liquid is gets heated, these bubbles emerge out slowly. This can also be attributed to the varying pore size in this case. In the nucleate boiling regime, a maximum frequency is observed during the isothermal phase on the vapor side. After this state, the bubble frequency decreases gradually. Some fluctuations are observed in case of higher heat load.

3.3.2 Bubble size

Bubble size is determined by finding the area occupied by each bubble in terms of pixels and these pixel values are converted in to diameter values from the calibrations performed during experiment. Subsequently, velocity of each bubble is also calculated by finding the number of frames each bubble takes to cross a fixed distance. This gives the time taken by a bubble to travel a fixed distance. The velocity determined above is the average bubble velocity. The bubble diameter is normalized with the average pore size (25µm). For all the visualization studies, a fixed area of 3mm x 3mm is considered.

Fig. 11 and fig.12 show variations of normalized bubble count (normalized with total number of bubbles) at each time instant with the normalized bubble sizes (normalized using nominal pore size) for heat loads of 60W and 40W respectively. The data shows variation of bubble sizes ranging from 4-11 times the nominal pore size of the wick. The most probable bubble size occurs around 7 times the nominal pore size. The distribution is similar for both heat loads.

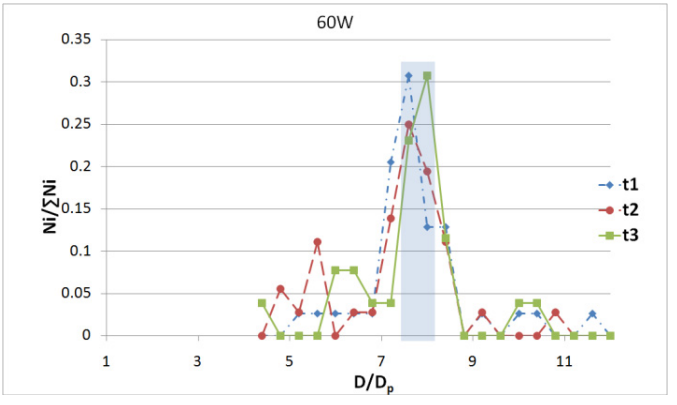

Fig. 11. Bubble size probability distribution function for 60W heat load

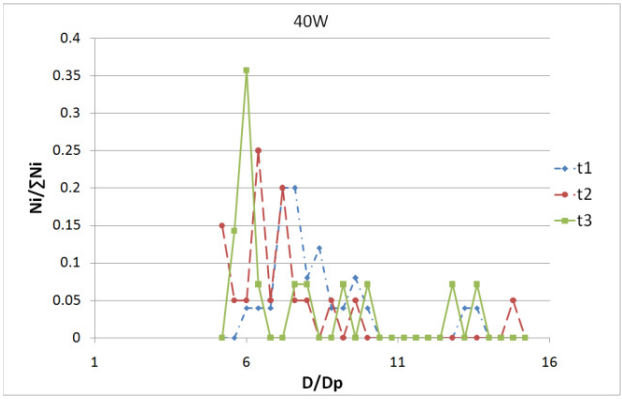

Fig. 12. Bubble size probability distribution function for 40W heat load

3.3.3 Bubble velocity

From the bubble diameter versus velocity plot (fig. 13), it can be concluded that the majority of bubbles have velocity around 30-60 mm/sec for the bubble of size 5-10 times the pore size. For 60W heat load, the cluster of points is distributed where as for 40W this band is narrow. The trend is mostly linear.

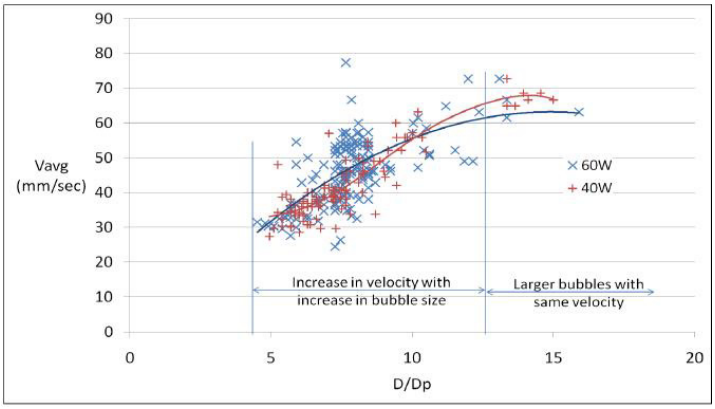

Fig. 13. Bubble velocity vs. relative size plot for 60W and 40

Conclusion

Evaporator region of flat plate loop heat pipe has been experimentally studied at different heat loads in the context of solar thermal applications. Temperatures are evaluated at different locations for calculation of heat transfer coefficient across the wick and bubbles are visualized in the CC. We can conclude that;

1. At higher heat loads of 40 and 60W temperature profiles depict two distinct regimes namely, convective heating and nucleate boiling, however, for 30W heater power only convective boiling regime is observed. So, there exists a critical heat load where the nucleate boiling commences in LHP. Hence, it is essential to operate LHP above this critical heat load for better performance.
2. As the heat loads increase the bubble size and velocity increases transmitting higher heat loads and so bubble dynamics have significant implications on heat transfer coefficient. Knowing the bubble dynamics, we can define the failure modes of the LHP.
3. Observed variation in heat transfer coefficients in different heating regimes and at different heater powers.
4. Mathematical correlations relating bubble dynamics and temperature field to heat load and performance of loop heat pipe have to be developed for full LHP setup.

References

[1] Mathioulakis E, Belessiotis V. A new heat-pipe type solar domestic hot water system. Solar Energy 2002;72(1):13-20.
[2] Chun W, Kang YH, Kwak HY, Lee YS. An experimental study of the utilization of heat pipes for solar water heaters 1999;19:807-817.
[3] Huang BJ, Lee JP, Chyng JP. Heat-pipe enhanced solar-assisted heat pump water heater. Solar Energy 2005;78(3):375-381.
[4] Singh R, Akbarzadeh A, Mochizuki M. Operational characteristics of a miniature loop heat pipe with flat evaporator. International Journal of Thermal Sciences 2008;47:1504-1515.
[5] Pastukhov VG, Maydanik YF. Low-noise cooling system for PC on the base of loop heat pipes. Applied Thermal Engineering 2007;27:894–901.
[6] Adoni AA, Ambirajan A, Vaidya JS, Kumar D, Dutta P. Theoretical and experimental studies on an Ammonia based loop heat pipe with a flat evaporator. IEEE TCPMT 2010;33(2):478-487.
[7] Wong SC, Chen CW. Visualization and evaporator resistance measurement for a groove-wicked flat-plate heat pipe. International journal of Heat and Mass Transfer 2012;55: 2229–2234.
[8] Muraoka I, Ramos FM, Vlassov VV. Analysis of the operational characteristics and limits of a loop heat pipe with porous element in the condenser. IJHMT 2001;44: 2287-2297.
[9] Lin G, Li N, Bai L, Wen D. Experimental investigation of a dual compensation chamber loop heat pipe. International journal of Heat and Mass Transfer 2010;53:3231-3240.
[10] Fukusako S, Komoriya T, Seki N. An experimental study of transition and film boiling heat transfer in liquid-saturated porous bed. Journal of heat transfer 1986;108:117-124.